Elucidating the Molecular Basis of Avibactam Mediated Inhibition of Class A β–Lactamases

Chandan Kumar Das[†,‡] and Nisanth N. Nair[*,†]

†*Department of Chemistry, Indian Institute Of Technology Kanpur, Kanpur, 208016, India*

‡*Current Address: Lehrstuhl für Theoretische Chemie, Ruhr Universität Bochum, 44780, Germany*

E-mail: nnair@iitk.ac.in

Abstract

Disseminating antibiotic resistance rendered by bacteria against the widely used $\beta-$lactam antibiotics is a serious concern in the public health care. Development of inhibitors for drug-resistant $\beta-$lactamase enzymes is vital to combat this rapidly escalating problem. Recently, the Food and Drug Administration has approved a non-β-lactam inhibitor called avibactam for the treatment of complicated intra–abdominal and urinary tract infections caused by drug–resistant Gram–negative bacteria. This work sheds light on the molecular origin of the inhibitory effect of avibactam against drug-resistant CTX–M variant of Class-A β–lactamase. Especially, we probed the structural evolution, dynamical features and energetics along the acylation and the deacylation reaction pathways through reliable enhanced sampling molecular dynamics methods and free energy calculations. We scrutinize the roles of active site residues, the nature of the carbonyl linkage formed in the inhibitor–enzyme covalent intermediate and other structural features of the inhibitor molecule. While unraveling the reasons behind the inhibition of all the deacylation routes, this study explains various experimental

structural and kinetics data, and paves the way to design new inhibitors based on the β-lactam framework.

1 Introduction

β–Lactam antibiotics are antibacterials that are routinely used to inhibit the bacterial cell–wall synthesizing enzymes known as penicillin binding proteins (PBPs). It is now well established that their clinical efficacy is progressively deteriorating due to the emergence of drug–resistance in bacteria, primarily associated with their expression of β–lactamases.[1,2] These enzymes hydrolyze β-lactam antibiotics in an efficient manner, preventing the drug molecules to react with PBPs. Four major classes of β–lactamases have been identified: A, B, C and D.[3] Among them, classes A, C and D β–lactamases use their active site serine residue for the catalysis, while class B β–lactamase employs either single zinc ion, or two zinc ions. Here, we focus on class–A serine β–lactamases (ABL). This particular class of β–lactamase includes extended-spectrum β–lactamases (such as SHV, TEM and CTX–M) and serine carbapenemases (for e.g. KPC), that are largely responsible for major outbreaks of antibiotic resistance.[1,4,5]

Mechanistically, the inactivation of β–lactam antibiotics by A, C and D β–lactamases occurs through two distinct chemical steps. In the first step (*viz.* acylation), the β–lactam drug reacts with the active site serine, resulting in the formation of a covalent drug–enzyme intermediate, which undergoes further hydrolysis (deacylation) in the next step and dissociates from the active site; see Figure 1. To restore the efficacy of β–lactam antibiotics, they are often prescribed in combination with slowly deacylating β–lactamase inhibitors. Amoxicillin-clavulanate, ticarcillin-clavulanate, ampicillin-sulbactam and piperacillin-tazobactam are some generally prescribed combinations of antibiotics and inhibitors.[6,7] These β–lactamase inhibitors contain reactive β–lactam core and they react with β–lactamase to form the inhibitor–enzyme covalent complex, similar to β–lactam antibiotics.

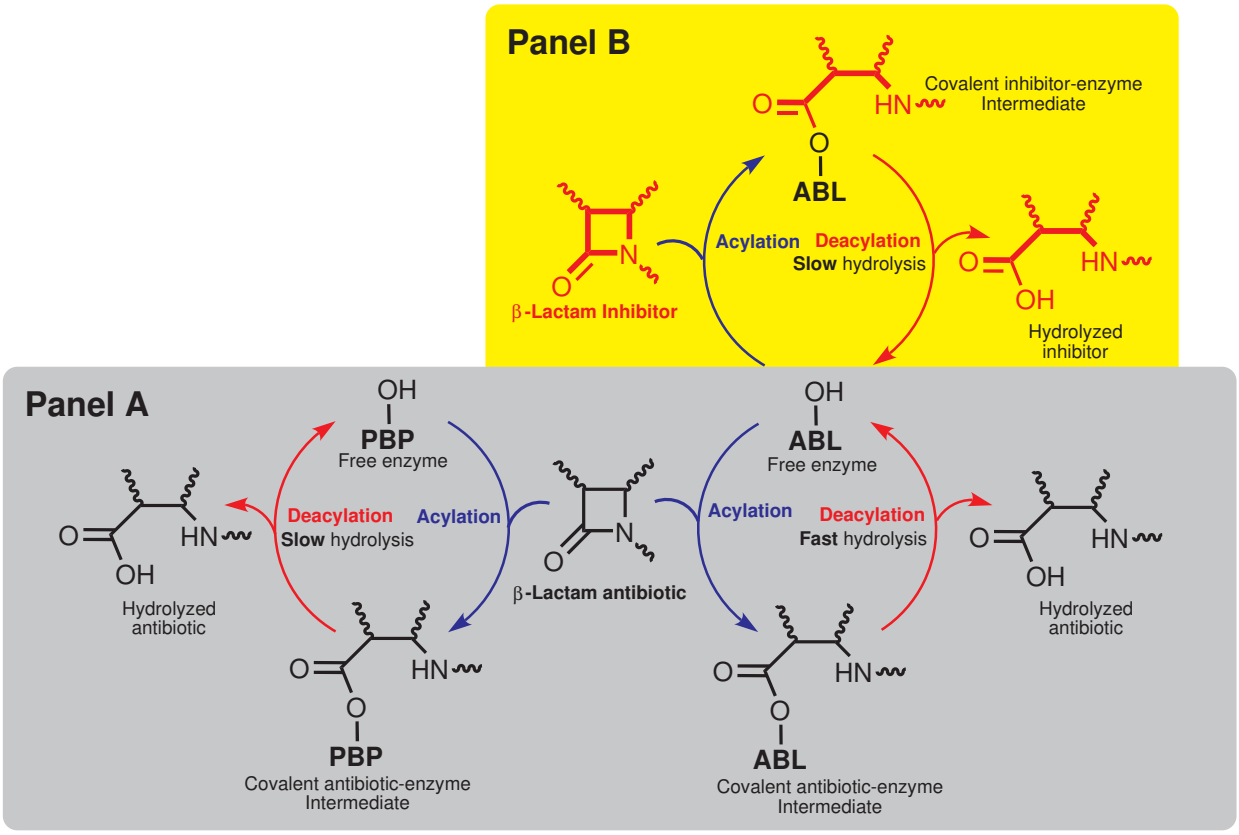

Figure 1: Panel A: mechanism of β–lactam antibiotic reaction with PBP and ABL. Panel B: mechanism of inhibition of ABL by β-lactam containing inhibitors.

Unlike β–lactam antibiotics, the inhibitor–enzyme covalent intermediate undergoes very slow deacylation, thereby deactivating these enzymes for longer time. Antibiotic–inhibitor combination therapy is reported to be effective against TEM and SHV variants of ABL, whereas CTX–M and KPC variant of ABL confer resistance against combination therapy.[6] Recently, the Food and Drug Administration (FDA) has approved a non–β–lactam inhibitor namely avibactam (or NXL104) for the treatment of complicated intra–abdominal and urinary tract infections together with ceftazidime (which is a third–generation cephalosporin family of β–lactam antibiotic).[8–12] Avibactam demonstrates exceptional inhibition against all classes of serine–reactive β–lactamases that includes TEM, SHV, CTX–M and KPC variant of ABLs.[8]

Akin to β–lactam inhibitors, avibactam acylates with β–lactamase enzyme and inhibits β–lactamase with nearly zero hydrolysis rate.[13,14] Interestingly, the abolition of hydrolysis

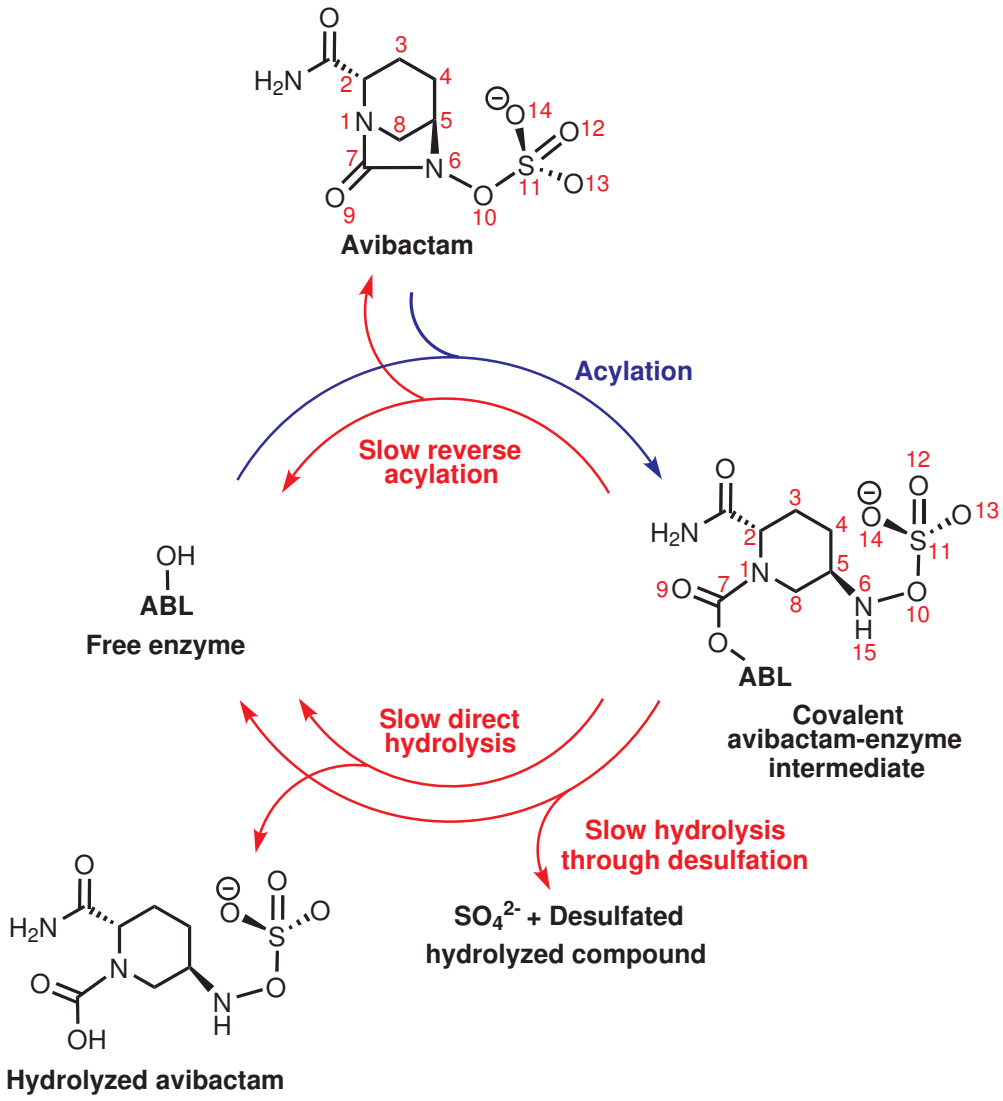

Figure 2: Potential mechanistic routes for avibactam mediated inhibition of ABL.

leads to cyclization of the ring–cleaved avibactam to its closed form through reverse acylation; see Figure 2.[15,16] In fact, this is also seen in the computational study on aztreonam (which is a β–lactam inhibitor) with class C β–lactamase.[17] Many other works further proposed mechanistic details of reverse acylation, considering it to be kinetically preferable over hydrolysis.[18–21] Based on point mutational studies[18,19] and high–resolution crystal structure captured by Lahiri *et al*,[20] a general base catalyzed mechanism is suggested for the recyclization of avibactam. Lahiri *et al*[20] hypothesized that the protonated form of the catalytic glutamate (Glu166) is unable to trigger the hydrolysis of the ring–opened avibactam and thus

the recyclization of avibactam is kinetically preferred. They further hypothesized a mechanism for recyclization in which deprotonated catalytic lysine (Lys73) accepts proton from N_6 through serine residue (Ser130), preceded by nucleophilic attack of N_6 on C_7. Computational study done by Schofield and co–workers scrutinized the recyclization of avibactam. However, they did not consider protonated Glu166 in their computational study.[22] On the other hand, Ehmann *et al* noticed slow hydrolysis of avibactam–enzyme covlent intermediate occurring through SO_4^{2-} release (see Figure 2), which could be a crucial observation in the understanding of avibactam mediated inhibition.[16] Similar observation was also reported by Shapiro *et al* in their kinetic and mass spectrometry experiments with another inhibitor of avibactam family (termed as ETX2514).[23] Our recent computational study on avibactam with class C β–lactamase shows that the desulfation (the release of SO_4^{2-}) process is an extremely slow process.[24] Further, the reverse acylation of ring–opened avibactam was found to be less likely. The kinetic stability of the covalent inhibitor–enzyme intermediate towards deacylation is key for the avibactam mediated inhibition.[24]

Understanding the genesis of slow deacylation of avibactam-ABL covalent complex could aid in the development of novel inhibitors. Despite of several biochemical and computational studies, molecular level understanding of the deacylation reaction remains elusive. We explore here various factors that can contribute to the sluggish deacylation reaction: (a) Reaction rates for deacylation via direct hydrolysis, reverse acylation, and desulfation.[24] (b) Steric occlusion of hydrolytic water at the active site;[24] (c) Retardation of hydrolysis of the acylated complex due to the chemical nature of the carbamoyl linkage. In order to address these, we performed extensive density functional theory (DFT) based hybrid quantum mechanics/molecular mechanics (QM/MM)[25] molecular dynamics (MD)[26] simulations beginning with the non–covalent CTX–M–15 and avibactam Michaelis complex. Enhanced sampling methods such as metadynamics[27,28] and well–sliced metadynamics[29] were employed to elicit inhibition mechanism and energetics. Finally, based on these computations, we propose plausible modifications to improve the efficacy of the existing β-lactam drugs.

2 Methods and Models

2.1 Simulation Setup and MM Simulation

Our starting structure of ABL:avibactam Michaelis complex (**ES**) was modeled from the crystal structure of CTX–M–15 (which is one of the extended-spectrum ABL) covalently bound with ring–opened avibactam (PDB ID 4HBU[20]). While modeling **ES**, the protonation state for all ionizable amino acids of the enzyme were set to their standard protonation state at pH= 7, except Lys73 and Glu166, which were considered to be in neutral form as suggested in earlier studies.[20,30–33] The Restrained Electrostatic Potential (RESP) derived point charges and the Generalized Amber force–field (GAFF)[34] for avibactam were obtained from our previous study.[24] The empirical parm99[35] version of Amber force–field was used for the protein molecule. The total charge of the system was neutralized by adding two Cl^- ions. The whole system was solvated by adding 10458 water molecules treated by TIP3P[36] force–field. The periodic simulation box has the dimensions 69×82×78 $Å^3$.

At first, we performed energy minimization using the MM force–field. While performing energy minimization, solvent molecules and hydrogens were only allowed to move first, but progressively the side chains and the whole protein were relaxed to obtain a good starting structure for the subsequent isobaric–isothermal NPT simulations. NPT runs were carried out at 1 atm and 300 K using Berendsen barostat[37] and Langevin thermostat.[38] A time–step of 1 fs was taken for integrating the equations of motion. Long range electrostatics was calculated by employing the particle-mesh Ewald(PME)[39] method and the non–bonded interaction cutoff is 15 Å. Within ∼2 ns of NPT simulation, we obtained reasonable convergence in the density. Thereafter, we performed NVT ensemble runs for 15 ns; see SI Figure S5 for protein backbone and active site RMSD monitored during the NVT simulation. The equilibrated **ES** structure obtained from NVT MM MD simulation was used for the successive QM/MM MD simulations.

2.2 QM/MM Simulation

We performed hybrid QM/MM simulation[25] using CPMD/GROMOS interface program, as available in the CPMD program package.[40] The catalytically relevant key active site residues (*viz.* Ser70, Lys73, Ser130, Glu166, Lys267) and avibactam molecule were included in the QM subsystem. An active site water molecule which could potentially involve in the catalysis was also included within the QM subsystem. We used the link atom scheme to treat the QM/MM boundary. The link atoms, which are hydrogen in this study, were kept constrained along the C_α–C_β bond for Ser/Glu residues, while they were placed between C_γ–C_δ bond for Lys; see SI Figure S6. The chosen QM simulation cell was cubic with a side length of 21 Å. We employed DFT level of theory and PBE[41] exchange and correlation functionals. Wavefunctions were expanded using plane wave basis set with a plane wave cut–off of 25 Ry and the core electrons were treated using Vanderbilt ultrasoft pseudopotentials.[42] Dynamics of the QM part was performed using the Car–Parrinello (CP) MD scheme.[43] In this case, the time step of integration was taken as 0.125 fs and the fictitious mass for the orbital degrees of freedom was assigned as 700 au. The electronic embedding scheme by Laio et al.[44] was employed to incorporate QM-MM interactions into the Hamiltonian. Separate Nosé-Hoover chains thermostats[45] were employed for nuclei and orbital degrees of freedoms. Temperature of the nuclear subsystem was set to 300 K, while that for the orbital degrees of freedom is close to 0 K. It is worth mentioning that all the atoms including the solvent molecules were relaxed during the QM/MM MD simulations.

2.3 Enhanced Sampling Techniques

In order to accelerate the sampling of chemical transformations and to estimate the associated free energy barriers, we employed metadynamics[27] approach within the framework of QM/MM MD. In this approach, a set of collective variables (CVs) that are vital to describe the chemical reaction of interest and accelerate conformational sampling are chosen. The CV dynamics is enhanced by introducing bias potential, that in turn facilitate the system to

escape from the current basin to the next basin in a self–guided fashion. For exploring flat and broad free energy basin in an efficient manner, we adopted well–sliced metadynamics[29] approach which is a combination of metadynamics and umbrella sampling on orthogonal CVs. Usually, umbrella sampling restraining potential[46] is activated along a CV where a controlled sampling is necessary, while the orthogonal CVs are enhanced sampled by well-tempered metadynamics.[47] The negative sum of bias potentials provides the underlying free energy surface in case of conventional metadynamics. On the other hand, appropriate re–weighting procedure[29,48] has been employed for reconstructing the free energy surface in the case of well–sliced metadynamics. We studied 11 elementary reaction steps and the length of the simulation for each case varied from 6 to 400 ps; see SI Table S1 and Section S1.

3 Results and Discussion

In order to obtain the overall kinetics of hydrolysis, it is crucial to compare the barrier of acylation, reverse acylation and deacylation reactions. Thus we looked these three set of reactions in a systematic manner and the results are presented in this section. Finally, we analyze the factors that affect the kinetic stability of the acyl-enzyme complex in the Discussion.

3.1 Acylation Reaction

Our study commences with the equilibration of **ES** structure employing MM and QM/MM simulations. Based on the previous studies,[20,30–33] we first considered Lys73 in deprotonated and Glu166 in protonated forms in the pre–catalytic **ES** structure. In the equilibrated structure, avibactam is nestled within the oxyanion hole comprised of backbone amide hydrogens of Ser70 and Ser237. In the equilibrated structure of **ES**, the neutral ϵ–amine of Lys73 is stably hydrogen bonded with the hydroxyl of nucleophile Ser70 (d[Lys73:$O_\zeta \cdots$ Ser70:H_γ] = 2.06±0.59 Å), suggesting that Lys73 could be the general base for the activation of Ser70

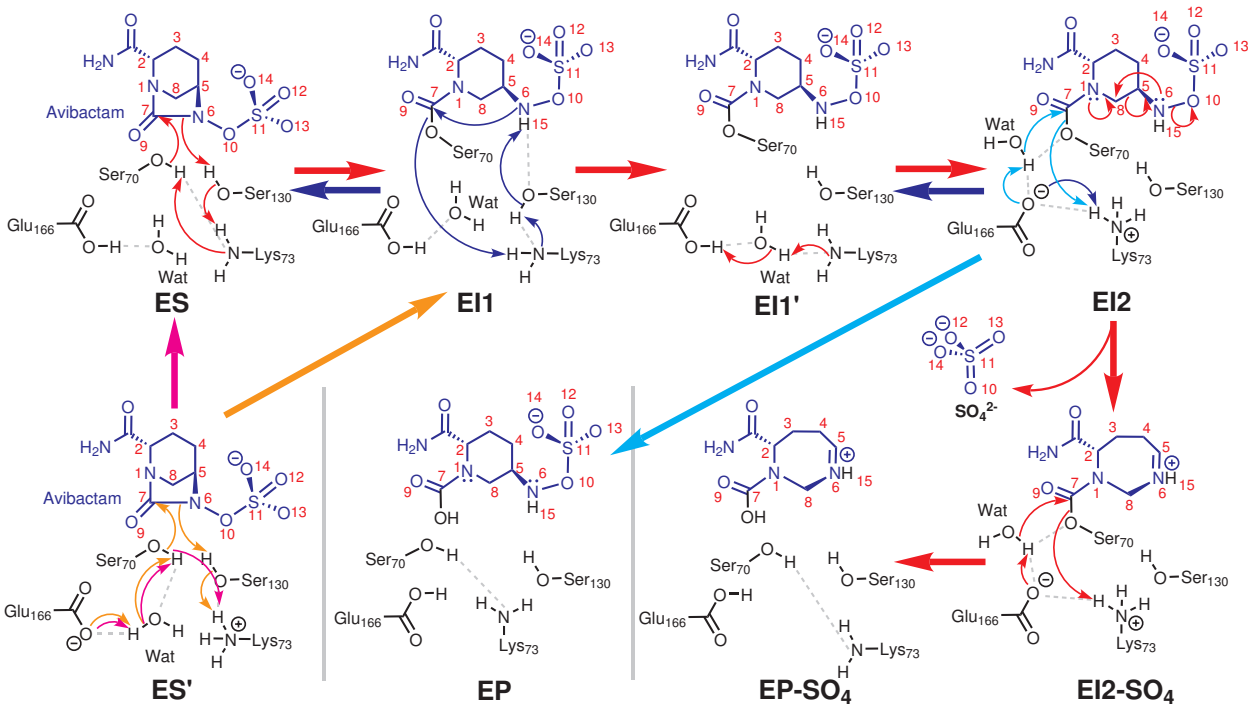

Figure 3: Mechanism of avibactam mediated inhibition of ABL elicited from our simulations. Some of the potentially crucial hydrogen bonds are shown in grey dotted lines.

in the acylation of avibactam. Hydrogen bonding interaction between Ser70 and Lys73 (deprotonated) was also noticed by Chen and co–workers in their high resolution X–ray crystal structure of enzyme–ligand non–covalent complex.[30] Besides that, the salt–bridge interaction between Arg268 and the sulfate group of avibactam and, the hydrogen bonding interactions between the side chain of active site asparagine residues (namely Asn98 and Asn126) and the amide group of avibactam stabilize the avibactam–enzyme Michaelis complex and provide suitable orientation to avibactam for the subsequent acylation reaction; see Figure 4 and SI Figure S7 for the equilibrated structure of **ES**.

Starting with the equilibrated structure of **ES**, we modeled the formation of avibactam–enzyme covalent intermediate through acylation reaction (**ES** $\rightarrow$ **EI1**); see Figure 3 and Figure 4. In this metadynamics simulation, the covalent bond formation in between Ser70:O_γ and carbonyl carbon (C_7) of avibactam, and the dissociation of C_7–N_6 bond were selected for enhance sampling. It is important to mention that these coordinates accelerate the chem-

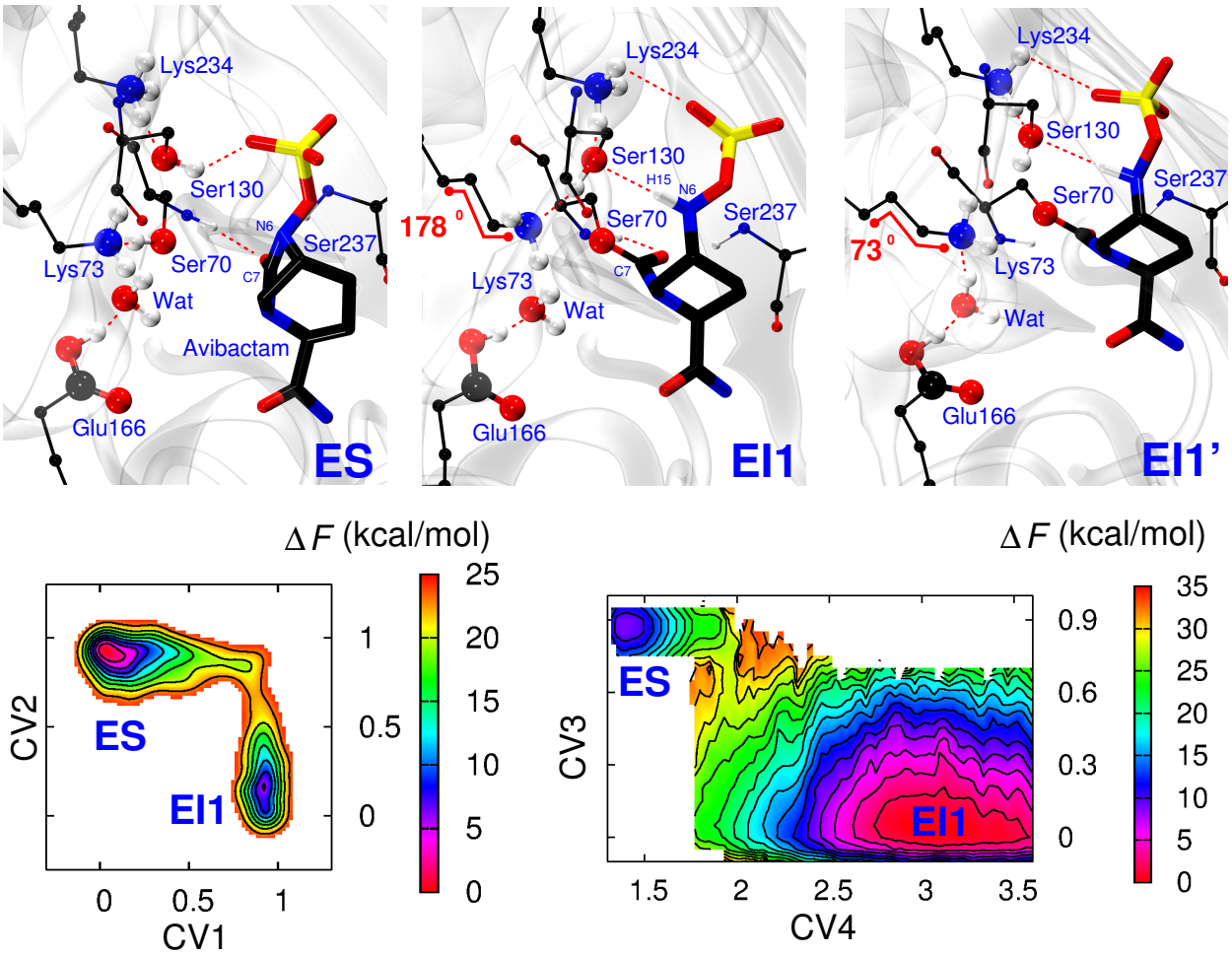

Figure 4: The equilibrated structure of **ES**, **EI1** and **EI1′** are displayed in the top panel, while the free energy surfaces for the **ES** → **EI1** (left) and the **EI1** → **ES** (right) reactions are displayed in the bottom panel. The CV labels are, CV1 is C[Ser70:O$_\gamma \cdots$ C$_7$], CV2 is C[N$_6 \cdots$ C$_7$], CV3 is C[Ser130:O$_\gamma \cdots$ H$_{15}$] and CV4 is d[N$_6 \cdots$ C$_7$]. Here C represents the coordination between two atoms (see SI Section S1 for definition of C). The avibactam molecule is shown in sticks model, while the catalytically relevant active site residues are shown in ball and stick representation. Atom color used here: C (black); N b(blue); O (red); S (yellow); H (white). Some of the crucial hydrogen bonding interactions are shown in the red dashed lines. The important atom levels are indicated in the figure. The dihedral C$_\gamma$–C$_\delta$–C$_\epsilon$–N$_\zeta$ of Lys73 determining **EI1** and **EI1′** intermediate is also indicated in the figure (in red color).

ical reaction in a chemically unbiased manner. Specific coordinates for (a) deprotonation of nucleophile (Ser70) prior to the ring–opening step, and (b) the protonation of N_6 after the ring–opening step were not chosen *a priori*. Moreover, no residue has been specifically attributed as a general base/acid, in order to capture the mechanism beyond chemical intuition.

With this setup, we could successfully observe the acylation reaction in our simulation, where the deprotonated Lys73 residue first abstracts the proton Ser70:H_γ. Subsequently, the activated Ser70 (Ser70:O_γ) attacks the carbonyl carbon center (C_7) of avibactam. As a result, the Ser70:O_γ–C_7 covalent bond is formed and concurrently the C_7–N_6 bond of avibactam is dissociated. This is accompanied by a spontaneous proton transfer from Lys73 to N_6 through Ser130 residue; see Figure 3. Such a mechanism was proposed earlier for β–lactam substrates.[31] The free energy barrier of **ES→EI1** reaction was computed to be 20 kcal mol^{-1} (Figure 8), and is reasonably close to the free energy barrier computed from experimental rates for acylation at 310 K (18 kcal mol^{-1}).[13,49]

To further ascertain the mechanism, we considered acylation reaction with Lys73 in protonated and Glu166 in deprotonated forms (**ES′**). This protonation state was earlier considered by Sgrignani *et al*[50] and Lizana *et al*[51] in their computational studies on the acylation of avibactam. Sgrignani *et al* proposed the Glu166 mediated activation of the nucleophile Ser70 where the deprotonated Glu166 activates the nucleophile Ser70 residue through an active site water molecule; see the **ES′** → **EI1** transformation in Figure 3. However, in the QM/MM study on acylation mechanism with β–lactam substrate, Mobashery and co–workers[31] showed that the Glu166 mediated activation is energetically unfavorable mechanistic route in comparison with the Lys73 mediated activation. Based on this, they discarded the Glu166 mediated activation mechanism and proposed an alternative mechanism in which the deprotonated Glu166 first takes a proton from the protonated Lys73 through the active site water molecule and Ser70. The reaction results in protonated Glu166 and deprotonated Lys73, and finally the deprotonated Lys73 activates the Ser70 residue; see

the mechanistic route of **ES′** → **ES** → **EI1** in Figure 3. On the other hand, Lizana *et al* suggested an asynchronous concerted mechanism of acylation in which the Ser70:H_γ directly transfers to N_6 after the nucleophilic attack of Ser70:O_γ on C_7. Here we studied all of these reaction mechanisms. Towards this, we carried out acylation of **ES′** using identical set of CVs as we used in the **ES** → **EI1** reaction. However, we did not observe the acylation reaction even after applying a bias potential of 30 kcal mol^{-1} in the reactant basin. This is a positive indication that the aforementioned reaction pathways are unlikely; see SI Section S2.

3.2 Deacylation Reaction

The potency of avibactam against β–lactamase carrying bacteria is crucially determined by the kinetic stability of the covalent intermediate **EI1**. Here we have investigated all potential degradation pathways of **EI1**; see Figure 2.

First, we modeled the cyclization of γ–lactam ring (**EI1** → **ES**, i.e. reverse-acylation) that leads to the regeneration of non–covalent Michaelis complex (**ES**); see Figure 3 and Figure 4. In the equilibrated structure of **EI1**, we note that neutral ϵ–amine Lys73 is hydrogen bonded with the hydroxyl of Ser130 (d[Lys73:$N_\zeta \cdots$ Ser130:H_γ] = 1.91±0.21 Å), which in turn is hydrogen bonded with H_{15} of the ring–opened avibactam (d[$H_{15} \cdots$ Ser130:O_γ] = 2.32±0.29 Å), indicating that Ser130 is likely to be the general base in **EI1** → **ES** reaction. In order to simulate the cyclization of γ–lactam ring, we performed well–sliced metadynamics, where the reformation of N_6–C_7 bond (*i.e.* γ–lactam ring–closure) was sampled by applying umbrella bias potentials, while the H_{15} abstraction from N_6 was accelerated by metadynamics bias. We observed the regeneration of the ring–closed avibactam in which deprotonated Lys73 abstracts the proton (H_{15}) from N_6 through Ser130. The N_6–C_7 bond reformation was accompanied with the breakage of the C_7–Ser70:O_γ bond. Finally, Lys73 transfers back a proton to Ser70:O_γ, thus completing **EI1**→**ES** transformation. The observed mechanism (Figure 3) is in line with the mechanism proposed by Lahiri *et al*[20] for the ABL catalyzed recyclization of avibactam. The point mutational studies by Winkler *et al*[18] and King *et al*[19]

reported that Ser130 acts as the base for the recyclization reaction, which is indeed in consensus with our simulation results. The free energy barrier for the recyclization (**EI1** $\rightarrow$ **ES**) was computed to be 29 kcal mol^{-1} (Figure 8), indicating that this process is an extremely slow process at ambient conditions.

As next, we probed the mechanism of degradation of the ring–opened avibactam through hydrolysis. Earlier computational study by Mulholland and co–workers[52] reported that the deprotonated Glu166 activates catalytic water (Wat), which in turn attacks carbonyl carbon of the covalent intermediate and hydrolyze the covalent bond between ABL and β–lactam drug molecule. However, in the case of avibactam, Lahiri *et al*[20] proposed that Glu166 remains protonated in the acyl–enzyme covalent intermediate (**EI1**). As a result, activation of deacylating water is impeded and slows down the hydrolysis of **EI1**. Clearly, deprotonation of Glu166 is a vital step in the deacylation reaction, although no previous studies have addressed it.

A structure–guided mechanistic study of CTX–M variant of ABL by Chen and co–workers[53] showed that notable conformational change of Lys73 and Glu166 dyad is taking place when the covalent intermediate is undergoing deacylation. In particular, the C_γ–C_δ–C_ϵ–N_ζ dihedral angle of Lys73 had been noticed to change from 175° (PBD ID 1YMS) to 77° (PBD ID 1YMX). As a consequence, the distance between Lys73:N_ζ and O_{Wat} (the oxygen of deacylating water molecule) decreased from 4.36 Å to 3.18 Å, while the distance between Glu166:O_ϵ and O_{Wat} remained nearly unchanged (2.50 Å $\rightarrow$ 2.46 Å),[53] suggesting that the deprotonation of Glu166 is likely to take place through proton transfer from protonated Glu166 to Wat, and subsequently Wat to deprotonated Lys73.

First, we modeled the formation of hydrogen bond between Lys73:N_ζ and H_{Wat} (proton of the deacylating water, Wat) accompanied by the breakage of Lys73:$N_\zeta \cdots$ Ser130:H_γ hydrogen bond (**EI1** $\rightarrow$ **EI1**$'$); see Figure 3 and Figure 5. We observed **EI1**$\rightarrow$**EI1**$'$ transformation takes place by overcoming a free energy barrier of 14 kcal mol^{-1}, whereas the corresponding reverse barrier is 9 kcal mol^{-1}; see Figure 8. As expected, the ϵ–amine of deprotonated

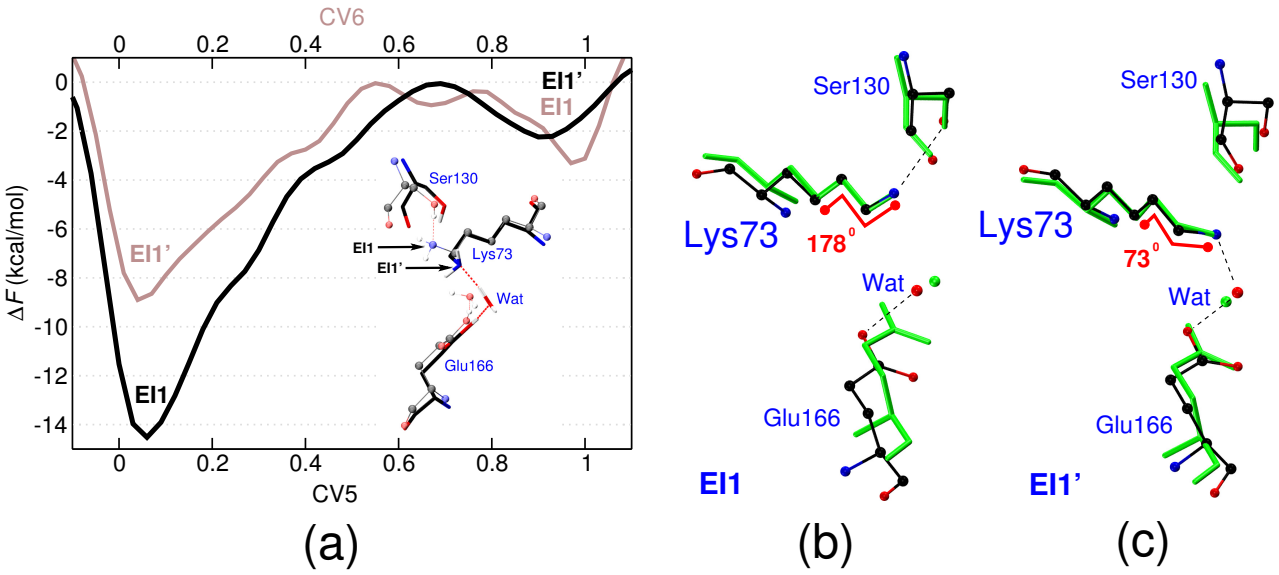

Figure 5: (a) The free energy surfaces for the **EI1** → **EI1′** transformation and its reverse transformation. The equilibrated structure of **EI1** (in ball–stick model) overlapped with the equilibrated structure of **EI1′** (in stick model) is shown in the inset figure. The ensemble averaged structures of **EI1** (b) and **EI1′** (c), both in ball–stick model, are overlapped with crystallographic structures (in stick model) PBD IDs 1YMS and 1YMX,[53] respectively.

Lys73 is hydrogen bonded with Wat, which in turn is hydrogen bonded with Glu166:H_ϵ in the equilibrated structure of **EI1′**; see Figure 5 (a). For further validation, we compared ensemble average structure of **EI1** and **EI1′** with the crystal structures of the acyl intermediates (PBD IDs 1YMS and 1YMX)[53] and we found striking structural similarity between them; see Figure 5 (b) and (c).

We then performed the **EI1′** → **EI2** reaction, where proton transfer from protonated Glu166 to deprotonated Lys73 takes place through Wat; see Figure 3 and Figure 6 (a). The dissociation of O_{Wat}–H_{Wat} and Glu166:O_ϵ–Glu166:H_ϵ were accelerated in this metadynamics simulation. The computed free energy barrier for this elementary step is 9 kcal mol^{-1} (Figure 8). We also observed the backward reaction (**EI2** → **EI1′**) occurring through proton transfer from protonated Lys73 to deprotonated Glu166 in a direct fashion; see Figure 3 and Figure 6 (b). The free energy barrier for this reaction was computed to be 4 kcal mol^{-1} (Figure 8), indicating that this proton transfer process is relatively fast at 300 K. It is

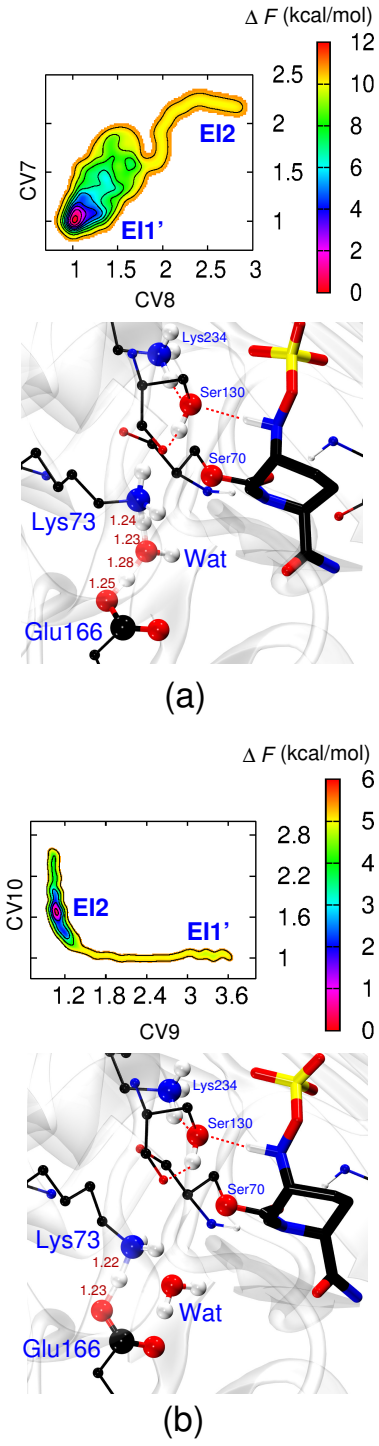

Figure 6: (a) A snapshot during **EI1′** → **EI2** transformation showing concerted proton transfer from Glu166 to Wat and from Wat to Lys73 is displayed in the bottom panel, whereas the free energy surface for the **EI1′** → **EI2** reaction is shown in the top panel. (b) A snapshot of showing direct proton transfer from Lys73 to Glu166 during the **EI2** → **EI1′** reaction is shown in bottom panel and the corresponding free energy surface is in the top panel. Crucial distances (in Å unit) are also indicated in the figure. Here, CV7 is d[$O_{Wat}\cdots H_{Wat}$], CV8 is d[Glu166:$O_\epsilon\cdots$Glu166:H_ϵ], CV9 is d[Lys73:$N_\zeta\cdots$Lys73:H_ζ] and CV10 is d[Glu166:$O_\epsilon\cdots$Lys73:H_ζ].

important to note that according to the computed free energy profile, the effective barrier for the deprotonation of Glu166 is far lesser than the barrier for the recyclization of avibactam, which tosses aside the hypothesis proposed by Lahiri *et al.*[20]

We continued our mechanistic investigations starting with the **EI2** intermediate obtained from the previous metadynamics simulation, and modeled Glu166 assisted hydrolysis of **EI2**, i.e. **EI2** $\rightarrow$ **EP**; see Figure 2 and Figure 3. For this, the nucleophilic addition of deacylating water (Wat) to carbonyl center (C_7) and the dissociation of Ser70:O_γ–C_7 covalent bond were chosen for enhance sampling. While **EI2** $\rightarrow$ **EP** transformation is taking place, the deprotonated Glu166 abstracts proton from Wat and then the activated Wat carries out the nucleophilic attack on C_7 of avibactam molecule; see Figure 3. At the same time, C_7 bond with Ser70:O_γ is cleaved, and immediately Ser70:O_γ takes proton from Lys73. In this manner, the **EI2** $\rightarrow$ **EP** transformation is completed and the active site is regenerated for the next catalytic cycle. The free energy barrier for **EI2**$\rightarrow$**EP** reaction was computed to be 41 kcal mol^{-1} (see SI Figure S2 and Figure 8). This is a very high free energy barrier and implies that the hydrolysis rate is nearly zero. We note in passing that during the hydrolysis of the avibactam–enzyme covalent complex, the deacylating water molecule attacks from the *re*–face of the carbonyl center. This is different to the nucleophilic attack in CBL,[24,54] where the water molecule approaches the *si*–face. Interestingly, in these cases, the axial –$NHOSO_3^-$ group (at the C_5 position) of the ring–opened avibactam hinders the entry of the deacylating water molecule to the active site, thereby inhibiting the hydrolysis.[24] Unlike in CBL, the axial –$NHOSO_3^-$ group in ABL is far from the deacylating water molecule. Therefore we find that the –$NHOSO_3^-$ group cannot occlude the approach of hydrolytic water.

We then investigated the mechanism and energetics of desulfation (SO_4^{2-} release) followed by slow hydrolysis which was initially put forward by Ehmann *et al*;[16] see Figure 3. In order to simulate the desulfation reaction, two mechanistically relevant events, namely dissociation of N_6–O_{10} and C_5–C_8 bonds, were enhanced sampled. We observed the fragmentation of SO_4^{2-} by the dissociation of N_6–O_{10} bond followed by an intra–molecular rearrangement

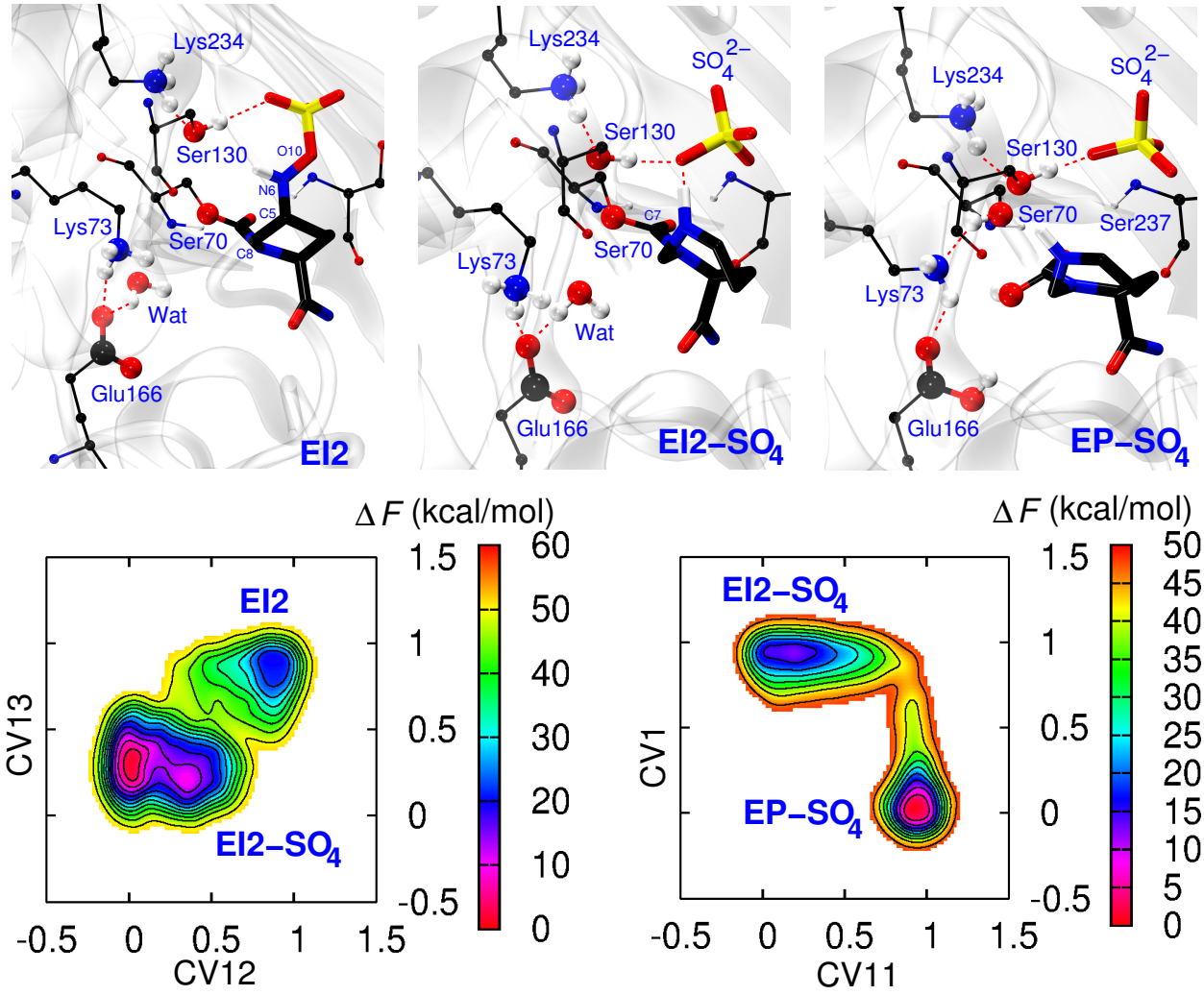

Figure 7: The equilibrated structure of **EI2**, **EI2**–$\mathbf{SO_4}$ and **EP**–$\mathbf{SO_4}$ are displayed in the top panel, while the free energy surfaces for the **EI2** → **EI2**–$\mathbf{SO_4}$ (left) and the **EI2**–$\mathbf{SO_4}$ → **EP**–$\mathbf{SO_4}$ (right) reactions are displayed in the bottom panel. The CV labels are, CV12 is $C[\mathrm{C_5 \cdots C_8}]$, CV13 is $C[\mathrm{N_6 \cdots O_{10}}]$, CV11 is $C[\mathrm{O_{Wat} \cdots C_7}]$ and CV1 is $C[\mathrm{Ser70{:}O_\gamma \cdots\ C_7}]$.

where N_6 makes a new bond with C_8 (**EI2** $\rightarrow$ **EI2–SO$_4$**). As a result, the six–membered ring is transformed to a seven–membered ring. The free energy barrier for the forward reaction is 29 kcal mol^{-1}, and that for the reverse reaction (**EI2–SO$_4$** $\rightarrow$ **EI2**) is more than 44 kcal mol^{-1}; see Figure 7 and Figure 8. The observed mechanism of desulfation and the computed free energy barrier for this process are in agreement with our previous investigation on avibactam mediated inhibition of CBL.[24]

Subsequently, we studied the hydrolysis of the desulfated avibactam derivative (**EI2–SO$_4$** $\rightarrow$ **EP–SO$_4$**); see Figure 3 and Figure 7. In this simulation, we employed same set of CVs as used in the simulation of **EI2**$\rightarrow$**EP** reaction. We observed that **EI2–SO$_4$**$\rightarrow$**EP–SO$_4$** transformation in our simulation where the reaction mechanism is identical to the **EI2**$\rightarrow$**EP** transformation. After completion of **EI2–SO$_4$**$\rightarrow$**EP–SO$_4$**, the active site recovered its native structure as in **ES**. The free energy barrier for **EI2–SO$_4$**$\rightarrow$**EP–SO$_4$** reaction was computed to be 34 kcal mol^{-1} (Figure 8). Upon release of the hydrolyzed and desulfated avibactam derivative into bulk water, it is likely to be subjected to further hydrolysis, which could result in CO_2 (or HCO_3^-) and a ketone compound with elemental composition $C_6H_{10}N_2O_2$, as found in experimental work of Ehmann *et al*;[16] see SI Figure S4 for a putative mechanism.

According to our computed free energy profile (see Figure 8), the effective barrier for direct hydrolysis (**EI1** $\rightarrow$ **EI1′** $\rightarrow$ **EI2** $\rightarrow$ **EP**) is comparatively higher than the barrier for the reverse acylation (**EI1** $\rightarrow$ **ES**). Similarly, the effective barrier along the **EI1** $\rightarrow$ **EI1′** $\rightarrow$ **EI2** $\rightarrow$ **EI2–SO$_4$** $\rightarrow$ **EP–SO$_4$** reaction route (39 kcal mol^{-1}) is higher than the reverse acylation (**EI1** $\rightarrow$ **ES**; 29 kcal mol^{-1}). This implies that the avibactam–β–lactamase covalent intermediate does not undergo direct hydrolysis, rather it undergoes slow recyclization leading to the formation of non–covalent Michaelis complex (**ES**). In this respect, our results are in line with the experimental observation reported by Ehmann *et al.*[15,16] Experimentally determined[16] deacylation rate constant (k_{off}) for wide varieties of ABLs including TEM–1, CTX–M–15 and KPC–2 are in the order of 10^{-4} (at 310 K), which corresponds to a free energy barrier of about 23 kcal mol^{-1}. This is in reasonably good agreement with the computed

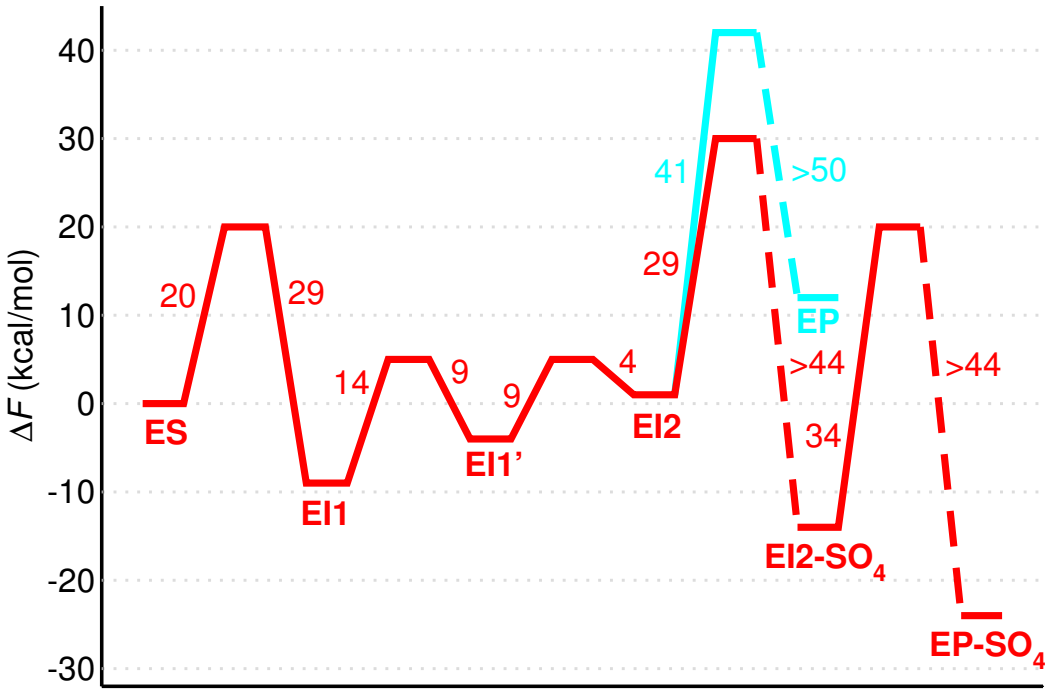

Figure 8: Complete free energy profile for avibactam mediated inhibition of ABL elicited in our simulations. Solid lines represent the free energy barriers computed from our calculations, while dotted lines indicate tentative free energy barriers.

barrier for recyclization of avibactam (29 kcal mol^{-1}). The significantly slow degradation of **EI1** intermediate is in agreement with the experimental observation of irreversible inhibition (with nearly zero depletion rate) accounted by Stachyra *et al*[13] and Xu *et al.*[14] Additionally, this also indicates that the **EI1** intermediate can be trapped in the crystallographic experiment. We compared the ensemble averaged equilibrated structure of **EI1** from our simulation with the existing crystal structure of avibactam bound ABL (PDB ID 4HBU[20]) and we find significant structural similarity between the two (see Figure 9). This further underpins the conclusion about the kinetic stability of the **EI1** intermediate. Altogether, avibactam covalently binds to the active site of ABL in the **EI1** state for a very long time and forestalls the catalytic activity of the enzyme.

The exceptionally high free energy barrier for the hydrolysis of enzyme–avibactam covalent bond is key to the inhibtion of ABL. To understand the origin of high free energy barrier for the hydrolysis reaction, we scrutinized the chemically distinctive carbamoyl link-

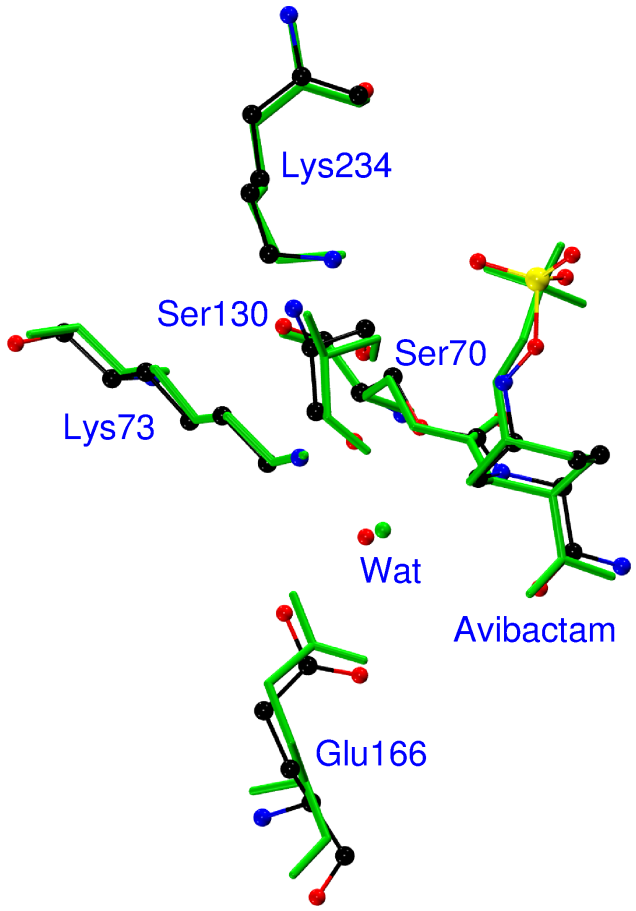

Figure 9: The ensemble averaged structure obtained from NVT simulation of **EI1** intermediate superimposed with the X–ray structure avibactam bound CTX–M–15 (PDB ID 4HBU[20]). The ensemble averaged structure is represented in ball–stick model, while the X–ray structure is shown in stick model (green color).

age present in the enzyme–avibactam covalent intermediate. We find a partial double bond character for the N_1–C_7 bond (d[N_1–C_7] = 1.37±0.02 Å), which in turn reduces the electrophilicity of C_7. This is leading to the retardation of the nucleophilic attack on C_7 by the deacylating water molecule that increases the reaction barrier (Figure 10). To validated this, we modified the original avibactam by mutating N_1 to carbon atom (C_1); see Figure 11 and SI Section S4. To some extent, this mimics the acyl linkage made by the conventional β–lactam substrates. Interestingly, we found that the barrier for the hydrolysis (**modEI2→modEP**) is decreased by 10 kcal mol^{-1}. This clearly indicates that N_1 (as part of the carbamoyl linkage) is indeed the basis for the exceptional hydrolytic stability of

avibactam–enzyme covalent intermediate. We think, this finding has important implication in deriving new inhibitors based on the molecular framework of β-lactam antibiotics (see Figure 11). This deserves detailed future studies.

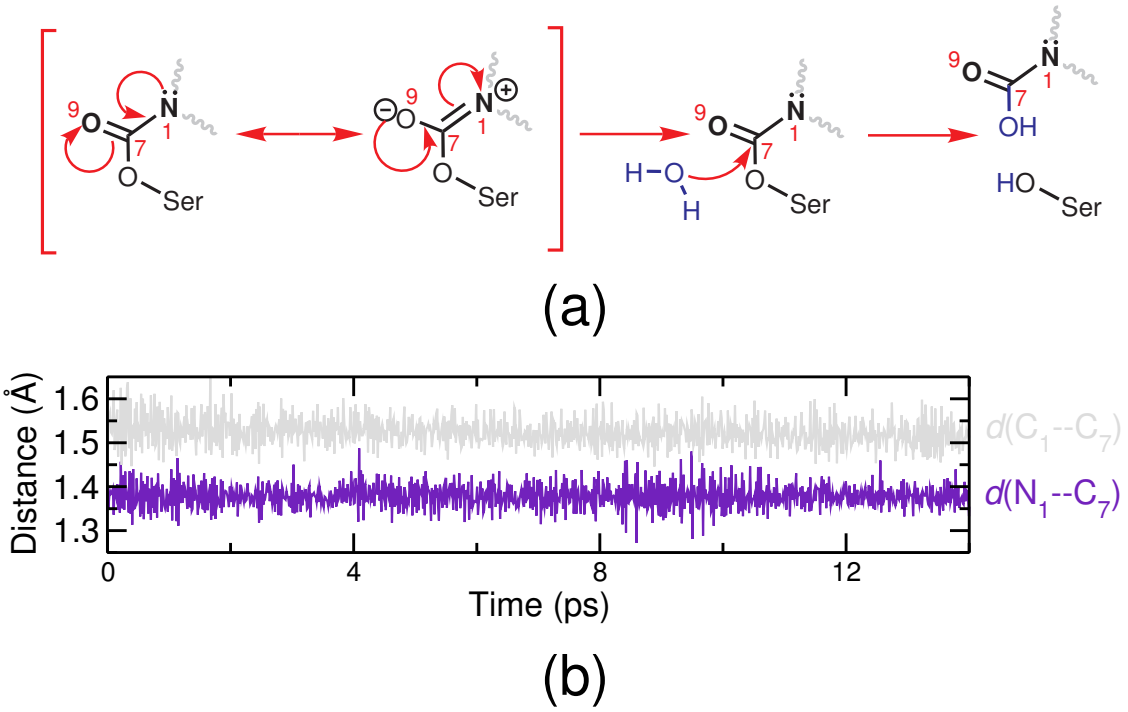

Figure 10: (a) The conjugative interaction between N_1 and carbonyl center (C_7) resulting in partial double bond character of N_1–C_7 bond in the carbamoyl linkage. (b) Time vs distance plot for the N_1–C_7 bond in the **EI2** intermediate and the C_1–C_7 bond in the **modEI2** intermediate.

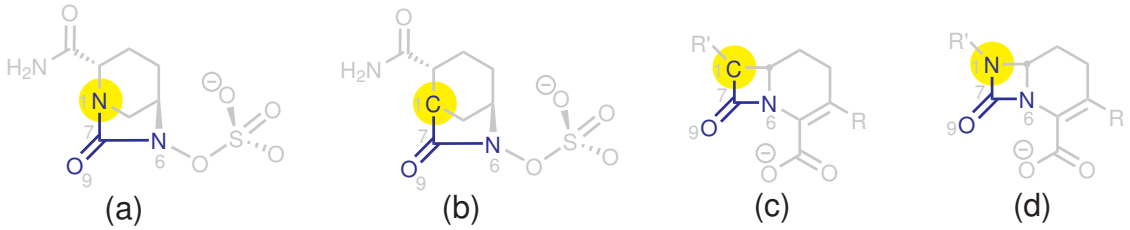

Figure 11: Chemical structure of avibactam (a), the modified avibactam which is studied here (b), the conventional β–lactam drug (c) and the modified β–lactam drug (d).

4 Conclusion

Through series of extensive DFT based QM/MM–metadynamics simulations, we have done a systematic investigation to unravel the molecular basis of inhibition of CTX–M variant of ABL by avibactam. Formation of avibactam:ABL covalent intermediate from the corresponding Michaelis complex is driven by the activation of Ser70 by Lys73. Moreover, Lys73 is aiding in protonating the substrate (N_6) during the ring-opening. Our simulations identified two stable acyl-enzyme intermediate structures and they agree remarkably well the intermediate structures observed in time revolved crystallographic study by Chen and co–workers.[53] We find that depletion of avibactam:ABL covalent intermediate cannot occur either through direct hydrolysis, or through irreversible release of SO_4^{2-}. Covalent intermediate rather undergoes very slow recyclization to non–covalent Michaelis complex and this explains the unusual reversible inhibition seen experimentally for avibactam.[13–16,18–20] We conclude that the significantly slow degradation of covalent intermediate is key to the inhibition of ABL by avibactam. Especially, the chemical nature of the carbomyl linkage in the covalent complex due to the N–atom is the molecular basis for this inhibiting property. This finding paves a way for the design of new inhibitor molecules based on the β-lactam framework.

Acknowledgement

The authors are thankful to IIT Kanpur for providing the HPC facility and the Department of Biotechnology, India, for funding this project. CKD thanks IIT Kanpur for his PhD scholarship.

References

(1) Bush, K. Bench-to-bedside review: The role of β-lactamases in antibiotic-resistant Gram-negative infections. *Critical Care* **2010**, *14*, 224.

(2) Bebrone, C.; Lassaux, P.; Vercheval, L.; Sohier, J.-S.; Jehaes, A.; Sauvage, E.; Galleni, M. Current Challenges in Antimicrobial Chemotherapy. *Drugs* **2010**, *70*, 651–679.

(3) Bush, K.; Jacoby, G. A.; Medeiros, A. A. A functional classification scheme for β–lactamases and its correlation with molecular structure. *Antimicrob. Agents Chemother.* **1995**, *39*, 1211–33.

(4) Bush, K. Alarming β–lactamase-mediated resistance in multidrug–resistant Enterobacteriaceae. *Curr. Opin. Microbiol.* **2010**, *13*, 558 – 564.

(5) WHO, *Antimicrobial resistance: global report on surveillance 2014*; WHO Press, World Health Organization: Geneva, 2014; http://www.who.int/drugresistance/documents/surveillancereport/en/ (accessed Oct, 2017).

(6) Drawz, S. M.; Bonomo, R. A. Three Decades of β–Lactamase Inhibitors. *Clin. Microbiol. Rev.* **2010**, *23*, 160–201.

(7) Shahid, M.; Sobia, F.; Singh, A.; Malik, A.; Khan, H. M.; Jonas, D.; Hawkey, P. M. Beta-lactams and Beta-lactamase-inhibitors in current- or potential-clinical practice: A comprehensive update. *Crit. Rev. Microbiol.* **2009**, *35*, 81–108.

(8) Coleman, K. Diazabicyclooctanes (DBOs): a potent new class of non–β–lactam β–lactamase inhibitors. *Curr. Opin. Microbiol.* **2011**, *14*, 550 – 555.

(9) Zhanel, G. G.; Lawson, C. D.; Adam, H.; Schweizer, F.; Zelenitsky, S.; Lagacé-Wiens, P. R. S.; Denisuik, A.; Rubinstein, E.; Gin, A. S.; Hoban, D. J. et al. Ceftazidime-

Avibactam: a Novel Cephalosporin/β–lactamase Inhibitor Combination. *Drugs* **2013**, *73*, 159–177.

(10) Wang, D. Y.; Abboud, M. I.; Markoulides, M. S.; Brem, J.; Schofield, C. J. The road to avibactam: the first clinically useful non-β-lactam working somewhat like a β-lactam. *Future Med. Chem.* **2016**, *8*, 1063–1084.

(11) Alatoom, A.; Elsayed, H.; Lawlor, K.; AbdelWareth, L.; El-Lababidi, R.; Cardona, L.; Mooty, M.; Bonilla, M.-F.; Nusair, A.; Mirza, I. Comparison of antimicrobial activity between ceftolozane–tazobactam and ceftazidime–avibactam against multidrug–resistant isolates of Escherichia coli, Klebsiella pneumoniae, and Pseudomonas aeruginosa. *J. Infect. Dis.* **2017**, *62*, 39 – 43.

(12) Wright, H.; Bonomo, R.; Paterson, D. New agents for the treatment of infections with Gram-negative bacteria: restoring the miracle or false dawn? *Clin. Microbiol. Infect.* **2017**, *23*, 704 – 712.

(13) Stachyra, T.; Péchereau, M.-C.; Bruneau, J.-M.; Claudon, M.; Frère, J.-M.; Miossec, C.; Coleman, K.; Black, M. T. Mechanistic Studies of the Inactivation of TEM-1 and P99 by NXL104, a Novel Non–β–Lactam β–Lactamase Inhibitor. *Antimicrob. Agents Chemother.* **2010**, *54*, 5132–5138.

(14) Xu, H.; Hazra, S.; Blanchard, J. S. NXL104 Irreversibly Inhibits the β–Lactamase from Mycobacterium tuberculosis. *Biochemistry* **2012**, *51*, 4551–4557.

(15) Ehmann, D. E.; Jahić, H.; Ross, P. L.; Gu, R.-F.; Hu, J.; Kern, G.; Walkup, G. K.; Fisher, S. L. Avibactam is a covalent, reversible, non–β–lactam β–lactamase inhibitor. *Proc. Natl. Acad. Sci.* **2012**, *109*, 11663–11668.

(16) Ehmann, D. E.; Jahić, H.; Ross, P. L.; Gu, R.-F.; Hu, J.; Durand-Réville, T. F.; Lahiri, S.; Thresher, J.; Livchak, S.; Gao, N. et al. Kinetics of Avibactam Inhibition against Class A, C, and D β–Lactamases. *J. Biol. Chem.* **2013**, *288*, 27960–27971.

(17) Awasthi, S.; Gupta, S.; Tripathi, R.; Nair, N. N. Mechanism and Kinetics of Aztreonam Hydrolysis Catalyzed by Class–C β–Lactamase: A Temperature-Accelerated Sliced Sampling Study. *J. Phys. Chem. B* **2018**, *122*, 4299–4308.

(18) Winkler, M. L.; Papp-Wallace, K. M.; Taracila, M. A.; Bonomo, R. A. Avibactam and Inhibitor-Resistant SHV β–Lactamases. *Antimicrob. Agents Chemother.* **2015**, *59*, 3700–3709.

(19) King, D. T.; King, A. M.; Lal, S. M.; Wright, G. D.; Strynadka, N. C. J. Molecular Mechanism of Avibactam-Mediated β–Lactamase Inhibition. *ACS Infect Dis* **2015**, *1*, 175–184.

(20) Lahiri, S. D.; Mangani, S.; Durand-Reville, T.; Benvenuti, M.; De Luca, F.; Sanyal, G.; Docquier, J.-D. Structural Insight into Potent Broad-Spectrum Inhibition with Reversible Recyclization Mechanism: Avibactam in Complex with CTX-M-15 and Pseudomonas aeruginosa AmpC β–Lactamases. *Antimicrob. Agents Chemother.* **2013**, *57*, 2496–2505.

(21) Lahiri, S. D.; Johnstone, M. R.; Ross, P. L.; McLaughlin, R. E.; Olivier, N. B.; Alm, R. A. Avibactam and Class–C β–Lactamases: Mechanism of Inhibition, Conservation of the Binding Pocket, and Implications for Resistance. *Antimicrob. Agents Chemother.* **2014**, *58*, 5704–5713.

(22) Choi, H.; Paton, R. S.; Park, H.; Schofield, C. J. Investigations on recyclisation and hydrolysis in avibactam mediated serine β–lactamase inhibition. *Org. Biomol. Chem.* **2016**, *14*, 4116–4128.

(23) Shapiro, A. B.; Gao, N.; Jahić, H.; Carter, N. M.; Chen, A.; Miller, A. A. Reversibility of Covalent, Broad-Spectrum Serine β-Lactamase Inhibition by the Diazabicyclooctenone ETX2514. *ACS Infect Dis* **2017**, *3*, 833–844.

(24) Das, C. K.; Nair, N. N. Molecular insights into avibactam mediated class C β–lactamase inhibition: competition between reverse acylation and hydrolysis through desulfation. *Phys. Chem. Chem. Phys.* **2018**, *20*, 14482–14490.

(25) Warshel, A.; Levitt, M. Theoretical studies of enzymic reactions: Dielectric, electrostatic and steric stabilization of the carbonium ion in the reaction of lysozyme. *J. Mol. Biol.* **1976**, *103*, 227 – 249.

(26) Marx, D.; Hutter, J. *Ab Initio Molecular Dynamics: Basic Theory and Advanced Methods.*; Cambridge University Press: Cambridge, 2009.

(27) Laio, A.; Parrinello, M. Escaping free-energy minima. *Proc. Natl. Acad. Sci.* **2002**, *99*, 12562–6.

(28) Iannuzzi, M.; Laio, A.; Parrinello, M. Efficient exploration of reactive potential energy surfaces using Car-Parrinello molecular dynamics. *Phys. Rev. Lett.* **2003**, *90*, 238302.

(29) Awasthi, S.; Kapil, V.; Nair, N. N. Sampling free energy surfaces as slices by combining umbrella sampling and metadynamics. *J. Comp. Chem.* **2016**, *37*, 1413–1424.

(30) Nichols, D. A.; Hargis, J. C.; Sanishvili, R.; Jaishankar, P.; Defrees, K.; Smith, E. W.; Wang, K. K.; Prati, F.; Renslo, A. R.; Woodcock, H. L. et al. Ligand-Induced Proton Transfer and Low-Barrier Hydrogen Bond Revealed by X–ray Crystallography. *J. Am. Chem. Soc.* **2015**, *137*, 8086–8095.

(31) Meroueh, S. O.; Fisher, J. F.; Schlegel, H. B.; Mobashery, S. Ab Initio QM/MM Study of Class–A β–Lactamase Acylation: Dual Participation of Glu166 and Lys73 in a Concerted Base Promotion of Ser70. *J. Am. Chem. Soc.* **2005**, *127*, 15397–15407.

(32) Tomanicek, S. J.; Standaert, R. F.; Weiss, K. L.; Ostermann, A.; Schrader, T. E.; Ng, J. D.; Coates, L. Neutron and X–ray Crystal Structures of a Perdeuterated Enzyme

Inhibitor Complex Reveal the Catalytic Proton Network of the Toho–1 β–Lactamase for the Acylation Reaction. *J. Biol. Chem.* **2013**, *288*, 4715–4722.

(33) Vandavasi, V. G.; Langan, P. S.; Weiss, K. L.; Parks, J. M.; Cooper, J. B.; Ginell, S. L.; Coates, L. Active-Site Protonation States in an Acyl-Enzyme Intermediate of a Class A β–Lactamase with a Monobactam Substrate. *Antimicrob. Agents Chemother.* **2017**, *61*, e01636–16.

(34) Wang, J.; Wolf, R. M.; Caldwell, J. W.; Kollman, P. A.; Case, D. A. Development and testing of a general amber force field. *J. Comp. Chem.* **2004**, *25*, 1157–1174.

(35) Cheatham, T. E.; Cieplak, P.; Kollman, P. A. A modified version of the Cornell et al. force field with improved sugar pucker phases and helical repeat. *J. Biomol. Struct. Dyn.* **1999**, *16*, 845–862.

(36) Jorgensen, W. L.; Chandrasekhar, J.; Madura, J. D.; Impey, R. W.; Klein, M. L. Comparison of simple potential functions for simulating liquid water. *J. Chem. Phys.* **1983**, *79*, 926–935.

(37) Berendsen, H. J. C.; Postma, J. P. M.; van Gunsteren, W. F.; DiNola, A.; Haak, J. R. Molecular dynamics with coupling to an external bath. *J. Chem. Phys.* **1984**, *81*, 3684–3690.

(38) Loncharich, R. J.; Brooks, B. R.; Pastor, R. W. Langevin dynamics of peptides: The frictional dependence of isomerization rates of N-acetylalanyl-N′-methylamide. *Biopolymers* **1992**, *32*, 523–535.

(39) Darden, T.; York, D.; Pedersen, L. Particle mesh Ewald: An Nlog(N) method for Ewald sums in large systems. *J. Phys. Chem.* **1993**, *98*, 10089–10092.

(40) `CPMD Version 3.12.04`, J. Hutter et al., IBM Corp 1990-2004, MPI für Festkörperforschung Stuttgart 1997-2001, see also `http://www.cpmd.org` (accessed by Oct, 2017).

(41) Perdew, J. P.; Chevary, J. A.; Vosko, S. H.; Jackson, K. A.; Pederson, M. R.; Singh, D. J.; Fiolhais, C. Atoms, molecules, solids, and surfaces: Applications of the generalized gradient approximation for exchange and correlation. *Phys. Rev. B* **1992**, *46*, 6671–6687.

(42) Vanderbilt, D. Soft self-consistent pseudopotentials in a generalized eigenvalue formalism. *Phys. Rev. B* **1990**, *41*, 7892–7895.

(43) Car, R.; Parrinello, M. Unified approach for molecular dynamics and density–functional theory. *Phys. Rev. Lett.* **1985**, *55*, 2471–2474.

(44) Laio, A.; VandeVondele, J.; Rothlisberger, U. A Hamiltonian electrostatic coupling scheme for hybrid Car-Parrinello molecular dynamics simulations. *J. Chem. Phys.* **2002**, *116*, 6941–6947.

(45) Martyna, G. J.; Klein, M. L.; Tuckerman, M. Nosé–Hoover chains: The canonical ensemble via continuous dynamics. *J. Chem. Phys.* **1992**, *97*, 2635–2643.

(46) Kumar, S.; Rosenberg, J. M.; Bouzida, D.; Swendsen, R. H.; Kollman, P. A. The weighted histogram analysis method for free–energy calculations on biomolecules. I. The method. *J. Comput. Chem.* **1992**, *13*, 1011–1021.

(47) Barducci, A.; Bussi, G.; Parrinello, M. Well-Tempered Metadynamics: A Smoothly Converging and Tunable Free-Energy Method. *Phys. Rev. Lett.* **2008**, *100*, 020603.

(48) Tiwary, P.; Parrinello, M. A Time–Independent Free Energy Estimator for Metadynamics. *J. Phys. Chem. B* **2015**, *119*, 736–742.

(49) Experimental barrier was calculated from the experimental rate constant for the reaction using the Eyring equation.

(50) Sgrignani, J.; Grazioso, G.; De Amici, M.; Colombo, G. Inactivation of TEM-1 by

Avibactam (NXL-104): Insights from Quantum Mechanics/Molecular Mechanics Metadynamics Simulations. *Biochemistry* **2014**, *53*, 5174–5185.

(51) Lizana, I.; Delgado, E. J. Theoretical insights on the inhibition mechanism of a class A Serine Hydrolase by avibactam. *J. Comp. Chem.* **2018**, *39*, 1943–1948.

(52) Hermann, J. C.; Ridder, L.; Höltje, H.-D.; Mulholland, A. J. Molecular mechanisms of antibiotic resistance: QM/MM modelling of deacylation in a class–A β–lactamase. *Org. Biomol. Chem.* **2006**, *4*, 206–210.

(53) Chen, Y.; Shoichet, B.; Bonnet, R. Structure, Function, and Inhibition along the Reaction Coordinate of CTX-M β–Lactamases. *J. Am. Chem. Soc.* **2005**, *127*, 5423–5434.

(54) Tripathi, R.; Nair, N. N. Deacylation Mechanism and Kinetics of Acyl–Enzyme Complex of Class–C β–Lactamase and Cephalothin. *J. Phys. Chem. B* **2016**, *120*, 2681–2690.

Graphical TOC Entry